RSC Advances

PAPER

View Article Online
View Journal | View Issue

Cite this: *RSC Adv.*, 2023, **13**, 18538

Investigation of the structure, phase transitions, molecular dynamics, and ferroelasticity of organic–inorganic hybrid $NH(CH_3)_3CdCl_3$ crystals

Ae Ran Lim *[ab]

Received 26th March 2023
Accepted 13th June 2023

DOI: 10.1039/d3ra01980b

rsc.li/rsc-advances

Understanding the physical and chemical properties of the organic–inorganic hybrid $NH(CH_3)_3CdCl_3$ is essential for its application. Considering its importance, a single crystal of $NH(CH_3)_3CdCl_3$ was grown with an orthorhombic structure at 300 K. The phase transition temperatures were determined to be 345 (T_{C3}), 376 (T_{C2}), and 452 K (T_{C1}) (phases IV, III, II, and I, respectively, starting from a low temperature). The partial decomposition temperature was 522 K (T_d). Furthermore, the NMR chemical shifts of the ^1H, ^{13}C, and ^{113}Cd atoms of the cation and anion varied with increasing temperature. Consequently, a significant change in the coordination geometry of Cl around Cd in $CdCl_6$ and a change in the coordination geometry of H in NH was associated with changes in the N–H···Cl hydrogen bond near the phase transition temperature. The ^{13}C activation energy E_a obtained from the spin-lattice relaxation time was smaller than that of ^1H E_a, suggesting that energy transfer around ^{13}C is easier. Additionally, a comparison of the twin domain walls measured *via* optical polarizing microscopy and Sapriel's theory indicated that the crystal structure in phase III was more likely to be orthorhombic than hexagonal.

1. Introduction

Until now, solar cells based on organic–inorganic hybrid materials have been extensively studied.[1–8] Typically, $CH_3NH_3PbX_3$ (X = Cl, Br, and I) materials are attracting attention as photovoltaic materials,[9–13] but these materials are easily degraded in a humid environment and are toxic due to the presence of Pb. Therefore, interest and research on eco-friendly organic–inorganic hybrid perovskite type materials have recently increased.[14–24] The development of solid-state physics has enabled the research on new materials with reduced- and low-dimensional properties. Alkylammonium groups can bond to inorganic groups *via* hydrogen bonding in various ways. Alkylammonium metal trihalogens, $NH(CH_3)_3MX_3$ (M = Cu, Co, Mn, Zn, or Cd; X = Cl or Br), have attracted considerable attention because of their low-order magnetic properties. These compounds exhibit structural phase transitions, which are considered to be due to the ordered–disorder-type orientation of the alkylammonium ions. Moreover, they exhibit interesting properties such as ferroelectricity, ferroelasticity, and low-dimensional magnetism.[25–28] These properties are related to the structural phase transitions that characterize these materials, including their potential applications in temperature and humidity sensors.[29,30]

$NH(CH_3)_3CdCl_3$ undergoes three phase transitions at 342, 374, and 415 K.[31] The four phases, ordered from low to high temperature, are referred to as phases IV, III, II, and I. According to previous reports by Chapuis *et al.*,[31–33] the low temperature phase IV (295 K) has an orthorhombic space group *Pbnm* structure, with lattice constants of $a = 8.986$ Å, $b = 14.502$ Å, $c = 6.710$ Å, and $Z = 4$. Additionally, the structure of phase III above 342 K is hexagonal, space group $P6_3/m$, with $a = 26.080$ Å, $c = 6.756$ Å, and $Z = 18$. Another hexagonal phase II between 374 K and 415 K, belongs to space group $P6_3/m$ with $a = 15.105$ Å, $c = 6.763$ Å, and $Z = 6$. Meanwhile, according to reports by Kashida *et al.*,[34–39] phase III belongs to the orthorhombic space group *Pbnm*, and has lattice parameters of $a = 17.123$ Å, $b = 15.256$ Å, $c = 6.731$ Å, and $Z = 8$, in contrast to the hexagonal structure reported by Chapuis *et al.*[31–33] The single-crystal structures in phase III reported by Chapuis *et al.*[31–33] and Kashida *et al.*[34–39] were orthorhombic and hexagonal, respectively. $NH(CH_3)_3CdCl_3$ comprises $[NH(CH_3)_3]^+$ and $[CdCl_6]^-$ octahedra. The atomic arrangement is connected by the alteration of organic cations and inorganic anions. Until now, relatively little attention has been paid to structural phase transitions.

In addition to the research on crystal structure described above, other studies on $NH(CH_3)_3CdCl_3$ have been conducted, including that of Sano and Kashida,[40] who investigated molecular reorientation using dielectric properties. Subsequently, Kchaou *et al.*[41–43] reported optical, electrical properties, IR, and Raman spectroscopy results.

The spin-lattice relaxation time ($T_{1\rho}$) in a rotating frame is generally mentioned as relaxation in the radio frequency field,

[a]*Graduate School of Carbon Convergence Engineering, Jeonju University, Jeonju 55069, Korea*

[b]*Department of Science Education, Jeonju University, Jeonju 55069, Korea. E-mail: aeranlim@hanmail.net; arlim@jj.ac.kr*

and is useful because it can provide information for slow motions of nuclei.[44,45] Ferroelasticity describes a phenomenon in which materials under external stress exhibit spontaneous strain induced by a phase transition between two equally stable phases, described mainly by lattice orientations. Consequently, ferroelastic materials respond to mechanical deformation by switching their phases with an accompanying lattice reorientation. Ferroelastic materials exhibit phase transitions between ferroelastic and paraelastic phases.[46]

Although the structures in phases IV, III, and II were reported, the crystal structure in phase III was not correct. And, the molecular dynamics studies have not been conducted for this material.

In this study, single crystals of $NH(CH_3)_3CdCl_3$ were grown using an aqueous solution method, and their structures were analyzed *via* single-crystal X-ray diffraction (XRD). Phase transition temperatures (T_C) were measured using differential scanning calorimetry (DSC) and powder XRD. In addition, the thermal stability that is not easily decomposed in a humid environment was discussed. To understand the role of the $NH(CH_3)_3$ cation and $CdCl_3$ anion in this crystal, the magic-angle spinning (MAS) nuclear magnetic resonance (NMR) chemical shifts for ^1H and ^{13}C, and static NMR chemical shifts for ^{113}Cd were obtained near the phase transition temperatures. Using this result, the role of the N–H···Cl hydrogen bond between the cation and anion was discussed. Furthermore, the spin-lattice relaxation time $T_{1\rho}$, which represents the energy transfer around the ^1H and ^{13}C atoms of the cation, was discussed, and their activation energies E_a were determined. To determine the exact structure in phase III, the existence of twin domains was suggested using polarizing microscopy and Sapriel's theory. The resulting crystal structure and physicochemical properties provide important information on the environment-friendly organic–inorganic hybrid for potential applications.

2. Experimental

2.1. Crystal growth

Single crystals of $NH(CH_3)_3CdCl_3$ were prepared from $NH(CH_3)_3Cl$ (Aldrich, 98%) and $CdCl_2$ (Aldrich, 98%) in a ratio of 1 : 1. The mixture was heated and stirred to obtain a homogeneous solution. The resulting solution was filtered, and transparent colorless single crystals with prismatic shapes elongated along the crystallographic *c*-axis were subsequently grown *via* slow evaporation after a few days at 300 K.

2.2. Characterization

The lattice parameters at 300 K were determined using single-crystal XRD at the Korea Basic Science Institute (KBSI) Western Seoul Center. Powder XRD patterns were measured at various temperatures in the same facility. The experimental conditions were similar to those reported previously.[47]

DSC measurements were performed using a DSC instrument (TA Instruments, DSC 25) in the temperature range of 200–573 K at heating and cooling rates of 10 °C min^{-1} under a flow of dry nitrogen gas. The amount of the sample used in the DSC experiment was 4.8 mg.

The ferroelastic twin domain wall observations were performed within a temperature range of 300–573 K using an optical polarizing microscope with a heating stage (Linkam THM-600).

Thermal gravimetric analysis (TGA) was also performed in the temperature range of 300–873 K with a heating rate of 10 ° C min^{-1} under nitrogen gas.

The MAS NMR spectra for ^1H and ^{13}C in the $NH(CH_3)_3CdCl_3$ crystals were measured using a solid-state 400 MHz NMR spectrometer (AVANCE III+, Bruker) at the KBSI Western Seoul Center. The ^1H NMR spectra were recorded at Larmor frequency of 400.13 MHz and ^{13}C NMR spectra were recorded at Larmor frequency of 100.61 MHz. The samples in the cylindrical zirconia rotors were spun at a rate of 10 kHz for the MAS NMR measurements to minimize the spinning sideband. The chemical shifts were referenced to adamantane and tetramethylsilane (TMS) for ^1H and ^{13}C, respectively, as standards for accurate chemical shift measurements. Spin-lattice relaxation time $T_{1\rho}$ values were obtained using a $\pi/2 - \tau$ pulse by a spin-lock pulse of duration τ for ^1H and ^{13}C, and were measured using a previously reported method.[48] Further, the ^{113}Cd static NMR spectra of the $NH(CH_3)_3CdCl_3$ crystals were measured at a Larmor frequency of 88.75 MHz, and the chemical shifts used $CdCl_2O_8 \cdot 6H_2O$ as standard samples. The chemical shifts and $T_{1\rho}$ could not be measured above 420 K because the NMR spectroscopy did not have adequate temperature control at high temperature. An almost constant temperature within the error range of ±0.5 K was maintained, even when the rate of flow of nitrogen gas and heater current were adjusted.

3. Results and discussion

3.1. Single-crystal XRD

Single-crystal XRD results for the $NH(CH_3)_3CdCl_3$ crystals were obtained at 300 K. The crystal grew an orthorhombic system with a *Pnma* space group and lattice constants of $a = 14.5088$ (8) Å, $b = 6.7108$ (3) Å, $c = 8.9901$ (4) Å, and $Z = 4$. These results at 300 K are consistent with those reported by Chapuis *et al.*[31–33] and Kashida *et al.*[34–39] Fig. 1 shows the thermal ellipsoids and

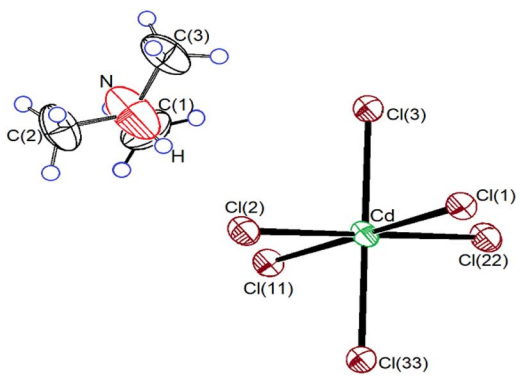

Fig. 1 Thermal ellipsoid plot (50% probability) for $NH(CH_3)_3CdCl_3$ crystal structure at 300 K.

Table 1 Crystal data and structure refinement for $NH(CH_3)_3CdCl_3$ at 300 K

Chemical formula	$C_3H_{10}NCdCl_3$
Weight	278.87
Crystal system	Orthorhombic
Space group	*Pnma*
T (K)	300
a (Å)	14.5088 (8)
b (Å)	6.7108 (3)
c (Å)	8.9901 (4)
Z	4
V (Å^3)	875.33
Radiation type	Mo-Kα
Wavelength (Å)	0.71073
Reflections collected	8940
Independent reflections	1173 ($R_{int} = 0.0441$)
Goodness-of-fit on F^2	1.073
Final R indices [$I > 2$ sigma(I)]	$R_1 = 0.0357$, $wR_2 = 0.1028$
R Indices (all data)	$R_1 = 0.0412$, $wR_2 = 0.1220$

Table 2 Bond-lengths (Å) and bond-angles (°) for $NH(CH_3)_3CdCl_3$ at 300 K

Cd–Cl(1)	2.6307 (11)
Cd–Cl(2)	2.6707 (12)
Cd–Cl(3)	2.6394 (12)
Cd–Cl(11)	2.6307 (11)
Cd–Cl(22)	2.6707 (12)
Cd–Cl(33)	2.6394 (12)
N–C(1)	1.408 (12)
N–C(2)	1.433 (9)
N–C(3)	1.433 (9)
Cl(1)–Cd–Cl(3)	84.06 (4)
Cl(1)–Cd–Cl(2)	95.89 (4)
Cl(3)–Cd–Cl(2)	95.85 (4)
Cl(1)–Cd–Cl(11)	180.00
Cl(2)–Cd–Cl(22)	180.00
Cl(3)–Cd–Cl(33)	180.00
C(1)–N–C(3)	116.7 (6)
C(1)–N–C(2)	116.7 (6)
C(3)–N–C(2)	115.2 (10)

atomic numbering of the $NH(CH_3)_3CdCl_3$ crystals. The XRD data are presented in Table 1, and the bond lengths and angles are presented in Table 2. The structure consisted of infinite chains of face-sharing $CdCl_6$ octahedra, and the $[NH(CH_3)_3]^+$ ion was located in the space between the chains. This compound is characterized by the hydrogen bonds N–H···Cl connecting the organic $[NH(CH_3)_3]^+$ cation to the inorganic $[CdCl_6]^-$ anion. Owing to the relatively strong bonds, the $CdCl_6$ octahedra were slightly elongated in the direction of the bonded Cl atom.

3.2. Phase transition and powder XRD

The DSC result was obtained at a temperature range of 200–573 K, with heating and cooling speed of 10 °C min^{-1} and a powder sample of 4.8 mg within the capsule. Fig. 2 shows two strong endothermic peaks (376 and 452 K) and three weak endothermic peaks (345, 416, and 522 K) as a result of heating. Endothermic peaks reported by other groups were observed at

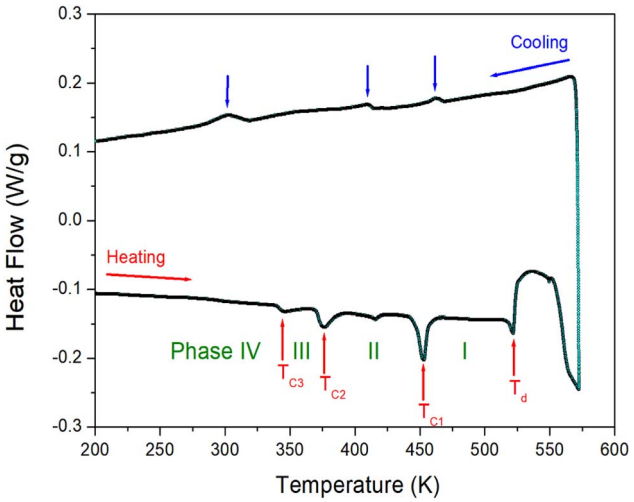

Fig. 2 Differential scanning calorimetry curve of $NH(CH_3)_3CdCl_3$ measured with the heating and cooling rates of 10 °C min^{-1}.

342, 374, and 415 K, whereas our results were observed at 345, 376, 416, 452, and 522 K. The enthalpies of the five peaks were 99, 377, 47, 717, and 370 J mol^{-1}, respectively. Furthermore, the exothermic peaks attributed to cooling were observed at 302, 409, and 462 K. The phase transition temperatures during heating and cooling were irreversible. From the DSC and the powder XRD results mentioned below, it was referred to as phase IV below 345 K, phase III between 345 and 376 K, phase II between 376 and 452 K, and finally phase I above 452 K.

The appearance of a single crystal according to the temperature change was observed using an optical polarizing microscope to confirm whether the five peaks shown in the DSC results in Fig. 2 are the phase transition temperatures or melting points. The crystals showed no significant changes until the temperature increased from 300 to 550 K. The surface of the single crystals began to melt at approximately 570 K.

Furthermore, a powder XRD experiment was performed using temperature change, and these results in the range of 8–70° (2θ) are shown in Fig. 3. As a comparison of experimental and theoretical simulation has been reported in many materials,[49–52] the theoretical XRD pattern at 300 K for $NH(CH_3)_3CdCl_3$ is shown in Fig. 3, which agrees well with the experimental pattern. The XRD patterns represented in blue (below 345 K) differ slightly from those recorded in olive (above 345 K); this difference is associated with T_{C3} (345 K). The XRD pattern recorded at 370 K differs from those obtained above 390 K (red), indicating a clear structural change ($=T_{C2}$). Furthermore, the XRD patterns below 452 K (red) differ from those recorded above 452 K (dark cyan), which is related to the T_{C1}. The change of the powder XRD peaks above 470 K is the result of the structural change by the phase transition temperature T_{C1}. The XRD patterns (dark cyan) below 522 K are different from those above 522 K (orange), which confirms that 522 K has a partial decomposition temperature T_d from the TGA experiment mentioned below. And, after observing the XRD patterns while heating up to 550 K, the XRD pattern (purple) did not

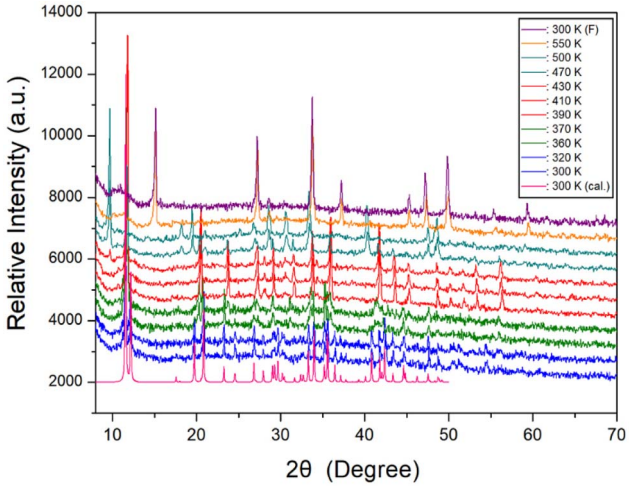

Fig. 3 Powder XRD patterns of $NH(CH_3)_3CdCl_3$ at phases IV, III, II, and I. T_d is XRD pattern at 550 K, 300 K (*F*) is XRD pattern at 300 K after heating to 550 K, and 300 K (cal.) is the theoretical XRD pattern at 300 K.

return to its original state after lowering the temperature. This was also confirmed by the XRD experiment that heating and cooling were irreversible in the DSC experiment. However, the XRD pattern for the small endothermic peak at 416 K shown in DSC experiment did not show any significant change. From the DSC, XRD, and polarizing microscopy experiments, the phase transition temperatures and the decomposition temperature were determined to be $T_{C3} = 345$ K, $T_{C2} = 376$ K, $T_{C1} = 452$ K, and $T_d = 522$ K, respectively.

3.3. Thermal property

TGA and differential thermal analysis (DTA) measurements were performed at the same 10 °C min^{-1} rate as in the DSC experiment, and the results are shown in Fig. 4. A colorless, transparent single crystal is shown in the inset of Fig. 4. The TGA results reveal that the crystal was thermally stable up to 530 K. The initial weight loss of $NH(CH_3)_3CdCl_3$ began at 530 K, representing the partial decomposetion temperature T_d with a weight loss of 2%. The T_d (=530 K) shown in the TGA result agrees well with the peak at 522 K shown in the DSC result. Therefore, it was confirmed that the endothermic peak at 522 K was T_d. The weight loss of approximately 34% at 640 K, which is at the largest inflection point in the TGA curve, was the result of the decomposition of $NH(CH_3)_3Cl$, an initial reagent in crystal growth. Around 870 K, the 55% weight loss is due to the decomposition of $NH(CH_3)_3Cl_2$, leaving almost only CdCl. The weight loss observed in the TGA experiment appears to agree well with the weight loss calculated from the chemical reaction. Near 973 K, $NH(CH_3)_3CdCl_3$ was completely decomposed. On the other hand, to confirm the phase transition temperatures, the DTA curve is shown in detail inside Fig. 7. T_{C1} and T_{C2} matched well with the peaks shown in DSC, and T_{C3} could be identified by the slope of the DTA curves indicated by the red line.

3.4. NMR chemical shifts and spin-lattice relaxation times for ^1H and ^{13}C

The NMR chemical shifts of ^1H in the $NH(CH_3)_3CdCl_3$ crystal were obtained in phases IV, III, and II, as shown in Fig. 5. The intensities of ^1H signals appeared to be small and large, respectively, in proportion to the number of H atoms in NH and CH_3. The ^1H chemical shifts for NH and CH_3 were 8.22 and 3.27 ppm, respectively, at 160 K and 7.72 and 3.24 ppm, respectively, at 410 K. As the temperature increased, the ^1H chemical shifts of CH_3 hardly changed, however, the ^1H chemical shifts of NH showed a large change compared to those of CH_3. This result indicates that the structural geometry around H, which is directly bound to N, changes significantly with temperature, although there is no rapid change near the phase-transition temperatures. The linewidths of ^1H in NH and CH_3 narrowed as the temperature increased, and those at 300 K were almost the same at 1.59 ppm.

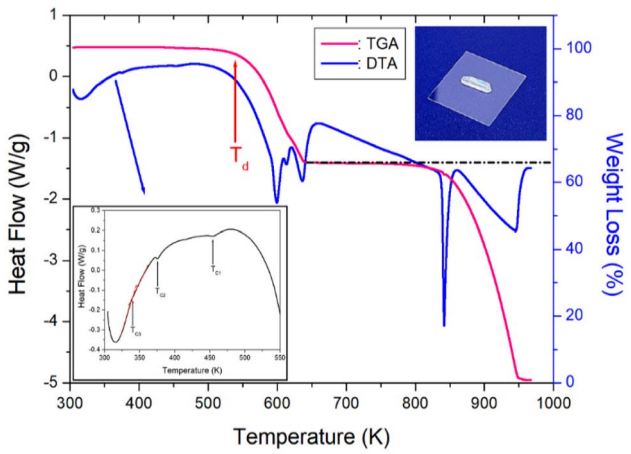

Fig. 4 Thermogravimetry and differential thermal analysis curves of $NH(CH_3)_3CdCl_3$ (inset: crystal shape of $NH(CH_3)_3CdCl_3$).

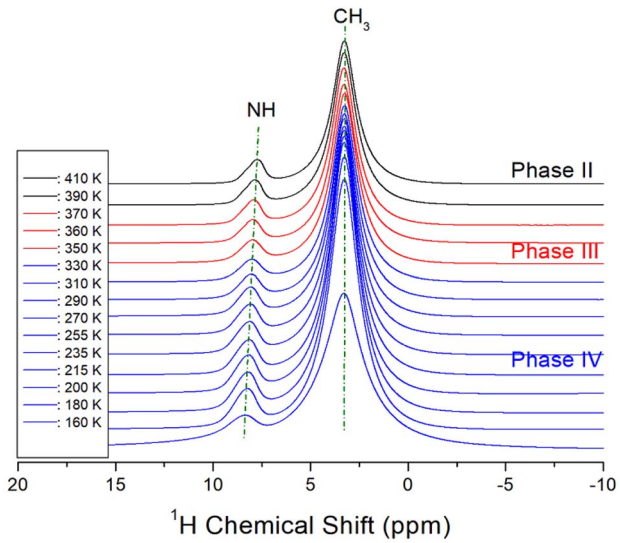

Fig. 5 *In situ* ^1H MAS NMR chemical shifts for $NH(CH_3)_3CdCl_3$ at phases IV, III, and II.

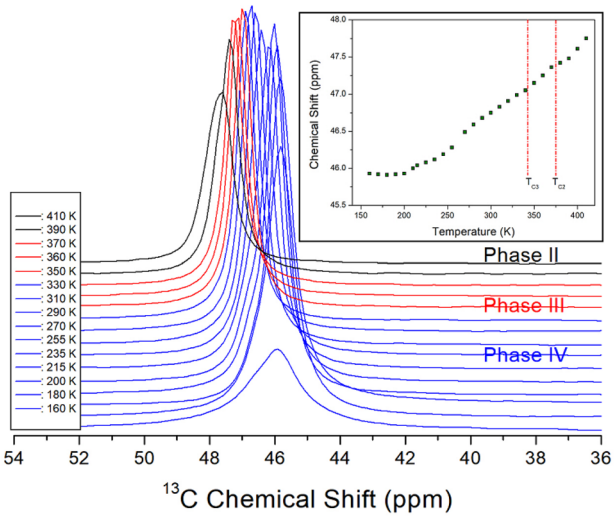

Fig. 6 *In situ* ^{13}C MAS NMR chemical shifts for $NH(CH_3)_3CdCl_3$ at phases IV, III, and II (inset: ^{13}C MAS NMR chemical shifts for $NH(CH_3)_3CdCl_3$ as a function of temperature).

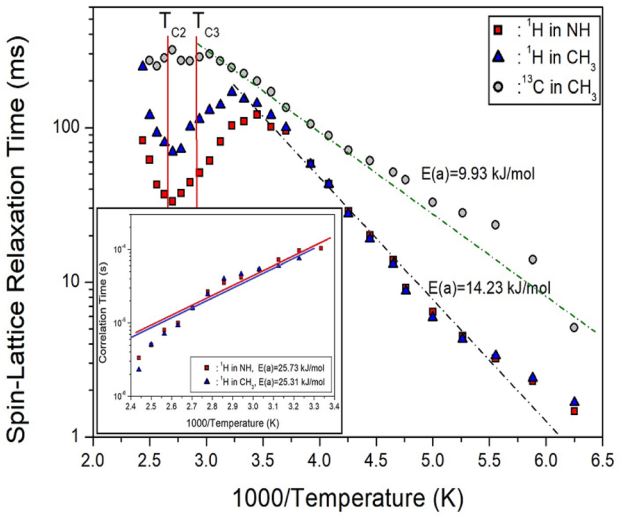

Fig. 7 ^{1}H and ^{13}C $T_{1\rho}$ of $NH(CH_3)_3CdCl_3$ as a function of inverse temperature, and the dot lines represent activation energies (inset: correlation times for ^{1}H at high temperature, and the solid lines represent activation energies).

The ^{13}C MAS NMR chemical shifts in $NH(CH_3)_3CdCl_3$ were also measured for phases IV, III, and II with increasing temperature, as shown in Fig. 6. Only one signal of ^{13}C for the three CH_3 ions shown in the crystal structure of Fig. 1 was recorded, thus, the structural environments of ^{13}C for the three CH_3 groups were all identical. At 300 K, a ^{13}C NMR chemical shift was observed at 46.74 ppm, and the line width was small at 0.68 ppm compared to the ^{1}H line width. As the temperature increased, the chemical shifts moved without any anomalous change, that is, the structural geometry of ^{13}C changed continuously with temperature. The ^{13}C NMR linewidths were narrower than the ^{1}H NMR linewidths for NH and CH_3, indicating that the molecular motion of ^{13}C located at the end of the $[NH(CH_3)_3]$ cation was significantly free.

The method to obtain $T_{1\rho}$ for ^{1}H and ^{13}C was to collect an FID following the spin-lock pulse. The intensity of the measured magnetization is given by:[44,45]

$$S(t)/S(0) = \exp(-\mathrm{TSL}/T_{1\rho}), \quad (1)$$

where $S(t)$ is the intensity of the resonance line at delay time t, $S(0)$ is the intensity of the resonance line at delay time $t = 0$, and TSL is the spin-lock pulse sequence. The experiment was repeated many times with different values of TSL, and the resulting intensities were used to find the value of $T_{1\rho}$. The $T_{1\rho}$ values for ^{1}H and ^{13}C in $NH(CH_3)_3CdCl_3$ were obtained using eqn (1) and the results are shown in Fig. 7 as a function of 1000/temperature. The ^{1}H and ^{13}C $T_{1\rho}$ values were strongly dependent on temperature, whereas, no special change occurred near the phase transition temperatures. The ^{1}H $T_{1\rho}$ values for NH and CH_3 increase rapidly as the temperature rises, and at a temperature above 300 K, the $T_{1\rho}$ values decrease as the temperature increases, reach a minimum value at 370 K, and then increase again. ^{1}H $T_{1\rho}$ values for NH and CH_3 are nearly similar below 300 K; however, at higher temperatures, ^{1}H $T_{1\rho}$ for CH_3 is greater than ^{1}H $T_{1\rho}$ for NH. At 370 K, the ^{1}H $T_{1\rho}$ values for CH_3 and NH are 69.62 and 33.28 ms, respectively, moreover, these are the minimum values for both, meaning molecular motion by the Bloembergen–Purcell–Pound (BPP) theory. The $T_{1\rho}$ minimum values are related to the reorientational motion of NH and CH_3. The experimental value of $T_{1\rho}$ is connected by the correlation time τ_C for molecular motion by the BPP theory, where the $T_{1\rho}$ value is given by:[53,54]

$$\begin{aligned}(1/T_{1\rho}) = R[&4J_1(\omega_1) + J_2(\omega_C - \omega_H) + 3J_3(\omega_C) \\ &+ 6J_4(\omega_C + \omega_H) + 6J_5(\omega_H)],\ J_1 = \tau_C/[1 + \omega_1{}^2\tau_C{}^2], \\ &J_2 = \tau_C/[1 + (\omega_C - \omega_H)^2\tau_C{}^2],\ J_3 = \tau_C/[1 + \omega_C{}^2\tau_C{}^2], \\ &J_4 = \tau_C/[1 + (\omega_C + \omega_H)^2\tau_C{}^2],\ J_5 = \tau_C/[1 + \omega_H{}^2\tau_C{}^2] \quad (2)\end{aligned}$$

where, R is a constant, ω_1 is the spin-lock field, and ω_C and ω_H are the Larmor frequencies for carbon and protons, respectively. The $T_{1\rho}$ minimum value was satisfied when $\omega_1\tau_C = 1$. The spin-lock field used in order to the obtain ^{1}H $T_{1\rho}$ was 62.5 kHz. The constant R value can be calculated by using τ_C obtained from $\omega_1\tau_C = 1$. Using the R, ω_1, ω_H, ω_C, and $T_{1\rho}$ obtained from the experiment, τ_C of molecular motion as a function of temperature was obtained. The local field fluctuation is described by the thermal motion of protons activated by thermal energy. The correlation time τ_C is represented as the Arrhenius dependence on the activation energy:[45,54]

$$\tau_C = \tau_C\,(0)\exp(-E_a/k_BT) \quad (3)$$

where $\tau_C\,(0)$, E_a, k_B, and T are the pre-correlation time, activation energy, Boltzmann constant, and temperature, respectively. The magnitude of E_a is related to molecular dynamics, and the plots of τ_C on a logarithmic scale *vs.* $1000/T$ for NH and CH_3 are shown in the inset of Fig. 7. It was found to be 25.73 ± 3.41 kJ mol^{-1} and 25.31 ± 2.45 kJ mol^{-1} for NH and CH_3, respectively, at high temperatures. Furthermore, the E_a for NH

and CH_3 at low temperatures was 14.23 ± 0.84 kJ mol^{-1}, and was obtained from the slope of the dotted line. The values of E_a at high temperatures were twice as high as those at low temperatures.

In the case of ^{13}C shown in Fig. 7, the $T_{1\rho}$ values increased rapidly as the temperature increased, and no significant change was seen at the phase transition temperatures. The behavior of the ^{13}C $T_{1\rho}$ for Arrhenius-type molecular motions that undergo fast motion can be represented as $\omega_1\tau_C \ll 1$, $T_{1\rho}{}^{-1} \sim \exp(E_a/k_BT)$, which is similar to the trend of ^1H $T_{1\rho}$ at low temperatures. The logarithmic scale of $T_{1\rho}$ *vs.* inverse temperature is represented by the dotted line in Fig. 7, where the activation energy for ^{13}C is $E_a = 9.93 \pm 2.58$ kJ mol^{-1}. The smaller E_a of ^{13}C compared to ^1H means that energy transfer around ^{13}C is less impeded.

3.5. Static NMR chemical shifts for ^{113}Cd

Because information can be obtained from the ^{113}Cd NMR chemical shifts, we attempted to consider changes in the structural environment around Cd in $CdCl_3$. The spin number of ^{113}Cd is $I = 1/2$, and only one resonance signal is expected.[55] *In situ* static ^{113}Cd NMR experiments as a function of temperature were employed to examine the structural environment of the $CdCl_6$ anions in $NH(CH_3)_3CdCl_3$, as shown in Fig. 8. The NMR chemical shifts were recorded using $CdCl_2O_8\cdot 6H_2O$ as the standard. The chemical shift of ^{113}Cd at 300 K was 240.36 ppm, and the linewidth was significantly broad at approximately 30 ppm. Unlike the ^1H and ^{13}C chemical shifts, the chemical shifts of ^{113}Cd changed between phases IV and III and phases III and II. This result indicates that the environment of the Cd atom surrounded by Cl atoms changed more in T_{C3} than in T_{C2}, unlike for ^1H and ^{13}C.

3.6. Ferroelastic property

The $NH(CH_3)_3CdCl_3$ crystal exists in four phases, and the crystal structure has been reported as follows: orthorhombic (*mmm*) in phase IV below 342 K, orthorhombic (*mmm*) or hexagonal (6/*mmm*) in phase III between 342 and 374 K, and hexagonal (6/*mmm*) in phase II above 374 K. If the structure is orthorhombic in phase III, ferroelastic twin domain walls should exist in phase III as 6/*mmmFmmm*, which is denoted by Sapriel's theory.[56] If the structure is hexagonal in phase III, twin domain walls should not exist in phase III, but domain walls should exist in phase IV. In other words, if phase III has an orthorhombic structure, twin domain walls in phase III should appear, as in the polarizing microscopy results. From the optical polarizing microscopy results, several parallel lines representing ferroelastic twin domain walls are present in phase III (Fig. 9(b)), and the domain pattern was not observed in phases IV and II (Fig. 9(a) and (c)). In phase IV, the domain walls did not appear, but in phase III, new domain walls began to appear from top to bottom. However, in Phase II, the domain walls disappeared and were not visible. The small lines seen in all the phases are not domain walls, as they appeared during the sample preparation for polarizing microscopy. For the transition from the *mmm* of the orthorhombic phase III to the 6/*mmm* of the hexagonal phase II, the equations on domain wall orientations were expressed as $x = 0$, $y = 0$, and $x = \pm\sqrt{3}$, $y = \pm\sqrt{3}$. According to Sapriel, the equations of the twin domain walls represent by the ferroelasticity of 6/*mmmFmmm*. Therefore, by comparing optical polarizing microscopy results and Sapriel's theory,[56] the crystal structures in phases IV, III, and II are more likely to be orthorhombic, orthorhombic, and hexagonal, respectively.

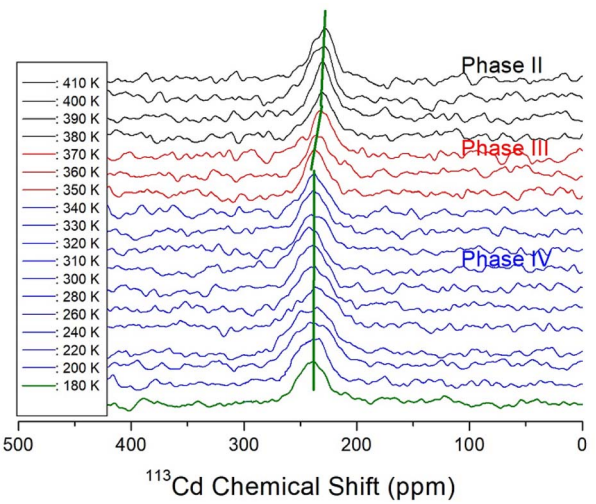

Fig. 8 *In situ* static ^{113}Cd NMR chemical shifts of $NH(CH_3)_3CdCl_3$ single crystal at phases IV, III, and II.

Fig. 9 The ferroelastic twin domain patterns at (a) phase IV, (b) phase III, and (c) phase II of $NH(CH_3)_3CdCl_3$ single crystal.

4. Conclusions

We analyzed the crystal structures, phase transition temperatures, thermal behavior, and structural dynamics of organic–inorganic hybrid $NH(CH_3)_3CdCl_3$ crystals to investigate their physicochemical properties. First, the orthorhombic structure of this crystal was confirmed using single-crystal XRD at 300 K, and the T_C values at 345, 376, and 452 K were determined using DSC and powder XRD. In addition, it was confirmed that the endothermic peak at 522 K was T_d. In the DSC results, the small peak at 415 K was observed in both the other groups[31–39] and our group, but it is thought to be due to impurities generated during crystal growth, not the phase transition temperature due to structural change. And, the crystal structure in phase III was more likely to be orthorhombic than hexagonal. Second, the chemical shifts were caused by the local field around the resonating nucleus. The ^1H, ^{13}C, and ^{113}Cd NMR chemical shifts of

the $[NH(CH_3)_3]$ cation and $[CdCl_6]$ anion varied with increasing temperature, suggesting that the surrounding environment changes with temperature. Changes in the ^{113}Cd NMR chemical shifts in $CdCl_6$ and ^1H NMR chemical shifts in NH were larger than those in the ^1H NMR chemical shifts in CH_3 and ^{13}C NMR chemical shifts in CH_3; ^1H and ^{13}C chemical shifts change continuously without rapid change according to temperature change, but ^{113}Cd chemical shifts in $CdCl_6$ show discontinuous changes near the phase transition temperatures. From this result, it was found that the surrounding environments of ^{113}Cd change more than those of ^1H and ^{13}C at the phase transition temperature. Also, the discontinuous change of Cd near the phase transition temperature is thought to induce the change of hydrogen bond N–H···Cl by the orientation of Cl around Cd. From these experimental results, it was found that the hydrogen bond N–H···Cl plays a significant role near the phase transition temperature. Additionally, $T_{1\rho}$, which represents the energy transfer around the ^1H and ^{13}C atoms of the cation, varied significantly with temperature. The smaller value of E_a for ^{13}C compared to ^1H suggests that energy transfer around ^{13}C is easier. Meanwhile, by comparing the twin domain walls using optical polarizing microscopy and Sapriel's theory, the crystal structure in phases IV, III, and II were found to likely be orthorhombic, orthorhombic, and hexagonal, respectively. The structural geometry revealed critical information regarding their basic mechanisms. Overall, this study elucidates these fundamental properties to broaden the applications of organic–inorganic hybrid compounds.

Conflicts of interest

There are no conflicts to declare.

Acknowledgements

This work was supported by the National Research Foundation of Korea (NRF) grant funded by the Korea government (MSIT) (2023R1A2C2006333). This research was also supported by the Basic Science Research Program through the National Research Foundation of Korea (NRF), funded by the Ministry of Education, Science, and Technology (2016R1A6A1A03012069).

References

1 S. K. Abdel, A. S. Abdel-Rahman, W. M. Gamal, M. AbdelKader, H. S. Ayoub, A. F. El-Sherif, M. F. Kandeel, S. Bozhko, E. E. Yakimov and E. B. Yakimov, *Acta Crystallogr., Sect. B: Struct. Sci., Cryst. Eng. Mater.*, 2019, **75**, 880.
2 Y.-F. Gao, T. Zhang, W.-Y. Zhang, Q. Ye and F. J. Da-Wei, *J. Mater. Chem. C*, 2019, **7**, 9840.
3 N. Mahfoudh, K. Karoui, F. Jomni and A. B. Rhaiem, *Appl. Organomet. Chem.*, 2020, **34**, e5656.
4 Y. Xie, Y. Ai, Y.-L. Zeng, W.-H. He, X.-Q. Huang, D.-W. Fu, J.-X. Gao, X.-G. Chen and Y.-Y. Tang, *J. Am. Chem. Soc.*, 2020, **142**, 12486.
5 D. -W. Fu, J.-X. Gao, W.-H. He, X.-Q. Huang, Y.-H. Liu and Y. Al, *Angew. Chem., Int. Ed.*, 2020, **59**, 17477.
6 C. Su, M. Lun, Y. Chen, Y. Zhou, Z. Zhang, M. Chen, P. Huang, D. Fu and Y. Zhang, *CCS Chem.*, 2021, **4**, 2009.
7 S. K. Abdel-Aal, M. F. Kandeel, A. F. El-Sherif and A. S. Abdel-Rahman, *Phys. Status Solidi A*, 2021, **218**, 2100036.
8 S. K. Abdel-Aal and A. Ouasri, *J. Mol. Struct.*, 2022, **1251**, 131997.
9 Q. Chen, N. D. Marco, Y. Yang, T.-B. Song, C.-C. Chen, H. Zhao, Z. Hong, H. Zhou and Y. Yang, *Nano Today*, 2015, **10**, 355.
10 I. M. Hermes, S. A. Bretschneider, V. W. Bergmann, D. Klasen, J. Mars, W. Tremel, F. Laquai, H.-J. Butt, M. Mezger, R. Berger, B. J. Rodriguez and S. A. L. Weber, *J. Phys. Chem.*, 2016, **120**, 5724.
11 E. Strelcov, Q. Dong, T. Li, J. Chae, Y. Shao, Y. Deng, A. Gruverman, J. Huang and A. Centrone, *Sci. Adv.*, 2017, **3**, e1602165.
12 S. K. Abdel-Aal, A. S. Abdel-Rahman, G. G. KocherOberlehner, A. Ionov and R. Mozhchil, *Acta Crystallogr., Sect. A: Found. Adv.*, 2017, **70**, C1116.
13 Y. Liu, L. Collins, R. Proksch, S. Kim, B. R. Watson, B. Doughty, T. R. Calhoun, M. Ahmadi, A. V. Ievlev, S. Jesse, S. T. Retterer, A. Belianinov, K. Xiao, J. Huang, B. G. Sumpter, S. V. Kalinin, B. Hu and O. S. Ovchinnikova, *Nat. Mater.*, 2018, **17**, 1013.
14 A. H. Mahmoudkhani and V. Langer, *Acta Crystallogr., Sect. B: Struct. Sci.*, 2002, **E58**, m592.
15 Z. Cheng and J. Lin, *CrystEngComm*, 2010, **12**, 2646.
16 M. F. Mostafa and S. S. El-khiyami, *J. Solid State Chem.*, 2014, **209**, 82.
17 S. Gonzalez-Carrero, R. E. Galian and J. Perez-Prieto, *Part. Part. Syst. Charact.*, 2015, **32**, 709.
18 S. K. Abdel-Adal, G. Kocher-Oberlehner, A. Ionov and R. N. Mozhchil, *Appl. Phys. A*, 2017, **123**, 531.
19 K. Pradeesh, G. S. Yadav, M. Singh and G. Vijaya Prakash, *Mater. Chem. Phys.*, 2010, **124**, 44.
20 S. Saikumar, J. J. Ahmad, G. Baumberg and G. Vijaya Prakash, *Scr. Mater.*, 2012, **67**, 834.
21 B. Staskiewicz, O. Czupinski and Z. Czapla, *J. Mol. Struct.*, 2014, **1074**, 723.
22 S. Ahmad, C. Hanmandlu, P. K. Kanaujia and G. Vijaya Prakash, *Opt. Mater. Express*, 2014, **4**, 1313.
23 Z. Czapla, J. Przeslawski, M. Crofton, J. Janczak, O. Czupinski, A. Ingram and M. Kostrzewa, *Phase Transitions*, 2017, **90**, 637.
24 H.-Y. Zhang, Z. Wei, P.-F. Li, Y.-Y. Tang, W.-Q. Liao, H.-Y. Ye, H. Cai and R.-G. Xiong, *Angew. Chem., Int. Ed.*, 2018, **57**, 526.
25 D. Visser, G. J. Mcintyre, W. G. Haje and W. J. A. Maaskant, *Phys. B*, 1989, **156–157**, 254.
26 J.-T. Yu, K.-T. Liu and Y.-H. Jeng, *Solid State Commun.*, 1994, **89**, 543.
27 A. Ben Rhaiem, N. Zouari, K. Guidara and A. Daoud, *J. Alloys Compd.*, 2005, **387**, 1.
28 Y. Zhang, H.-Y. Ye, W. Zhang and R.-G. Xiong, *Inorg. Chem. Front.*, 2014, **1**, 118.

29 H. Reshak, H. Kamarudir, I. V. Kityk and S. Auluck, *J. Mater. Sci.*, 2013, **48**, 5157.
30 K. Karoui, A. Ben Rhaiem, F. Jomni, J. L. Moneger, A. Bulou and K. Guidara, *J. Mol. Struct.*, 2013, **1048**, 287.
31 U. Walther, D. Brinkmann, G. Chapuis and H. Arend, *Solid State Commun.*, 1978, **27**, 901.
32 G. Chapuis and F. J. Zuniga, *Acta Crystallogr., Sect. B: Struct. Crystallogr. Cryst. Chem.*, 1980, **36**, 807.
33 G. Chapuis and F. J. Zuniga, *Acta Crystallogr., Sect. B: Struct. Sci.*, 1988, **44**, 243.
34 T. Fukumoto, K. Sano, S. Kashida and H. Kaga, *J. Phys. Soc. Jpn.*, 1983, **52**, 4213.
35 S. Kashida, K. Sano, T. Fukumoto, H. Kaga and M. Mori, *J. Phys. Soc. Jpn.*, 1983, **52**, 1255.
36 T. Fukumoto and S. Kashida, *J. Phys. Soc. Jpn.*, 1985, **54**, 3785.
37 S. Kashida and S. Sato, *J. Phys. Soc. Jpn.*, 1985, **54**, 2934.
38 S. Kashida, K. Sano, T. Fukumoto, H. Kaga and M. Mori, *J. Phys. Soc. Jpn.*, 1985, **54**, 211.
39 S. Kashida, Y. Ito and S. Sato, *J. Solid State Chem.*, 1987, **69**, 258.
40 K. Sano and S. Kashida, *J. Phys. C: Solid State Phys.*, 1987, **20**, 2985.
41 H. Kchaou, A. Ben Rhaiem, K. Karoui, F. Jomni and K. Guidara, *Appl. Phys. A*, 2016, **122**, 82.
42 H. Kchaou, K. Karoui, A. Bulou and A. Ben Rhaiem, *Phys. E*, 2017, **88**, 50.
43 H. Kchaou, K. Karoui and A. Ben Rhaiem, *Phys. E*, 2017, **85**, 308.
44 G. Heidi, *A Study of $T_{1\rho}$ Relaxation: From Relaxation Mechanisms to the Magnetic Resonance Imaging Contrast*, Kuopio University printing, Finland, 2003.
45 A. Abragam, *The Principles of Nuclear Magnetism*, Oxford University press, 1961.
46 E. K. H. Salje, *Ann. Rev. Mater. Res.*, 2012, **42**, 265.
47 A. R. Lim and J. Cho, *Sci. Rep.*, 2022, **12**, 16901.
48 A. R. Lim, *RSC Adv.*, 2021, **11**, 37824.
49 A. Bootchanont, S. Rujirawat, R. Yimnirun, R. Guo and A. Bhalla, *Ceram. Int.*, 2016, **42**, 8151.
50 M. Matsuki, T. Yamada, N. Yasuda, S. Dekura, H. Kitagawa and N. Kimizuka, *J. Am. Chem. Soc.*, 2018, **140**, 291.
51 X.-F. Zhou, A. R. Oganov, X. Dong, L. Zhang, Y. Tian and H.-T. Wang, *Phys. Rev. B: Condens. Matter Mater. Phys.*, 2011, **84**, 054543.
52 A. K. Singh and A. K. Singh, *Solid State Sci.*, 2012, **14**, 100.
53 R. K. Harris, *Nuclear Magnetic Resonance Spectroscopy*, Pitman Pub, UK, 1983.
54 J. L. Koenig, *Spectroscopy of Polymers*, Elsevier, New York, 1999.
55 S. Sakida and Y. J. Kawamoto, *J. Phys. Chem. Solids*, 2002, **63**, 151.
56 J. Sapriel, *Phys. Rev. B: Solid State*, 1975, **12**, 5128.